

## Study of the dynamics of magnetic particles in rotating magnetic field: A 3D finite element analysis

Jiangang Ku <sup>1</sup>, Xuyan Yu <sup>1</sup>, Jun Xia <sup>2</sup>, Qian Wang <sup>3</sup>, Zhaolian Wang <sup>3</sup>, Zhongyun Lei <sup>4</sup>

<sup>1</sup>Zijin School of Geology and Mining, Fuzhou University, Fuzhou, Fujian 350108, China

<sup>2</sup>School of Materials Science and Engineering, Fuzhou University, Fuzhou, Fujian 350108, China

<sup>3</sup>Shandong Huate Magnet Technology Co., Ltd., Weifang 261061, China

<sup>4</sup>College of Chemical Engineering, Fuzhou University, Fuzhou, Fujian 350108, China

Corresponding author: zhongyun\_lei@163.com (Zhongyun Lei)

**Abstract:** The analysis of magnetic particle dynamics in a rotating magnetic field and the exploration of the magnetic agglomeration mechanism are crucial for effectively reducing agglomeration in strong magnetic minerals and improving sorting efficiency. The forces acting on magnetic particles in a rotating magnetic field were analyzed in this study. A 3D model was built to simulate the complex interaction between two magnetic particles in a rotating magnetic field using COMSOL Multiphysics finite element simulation software. It shows that the number of periods of change in the spiral period, velocity, and acceleration remains consistent under different conditions. Additionally, their period numbers are positively correlated with magnetic field rotational speed, medium viscosity, and the initial particle spacing, and negatively correlated with magnetic field strength. Under various conditions, the larger the area of the velocity-closed surface in the same cycle, the larger the helical diameter of the particle trajectory. The initial acceleration of the particles exhibits a positive correlation with the strength of the magnetic field, a negative correlation with the viscosity of the medium and the initial distance, and no significant relationship with the rotational speed of the magnetic field. For further research on the dynamics of magnetic particles and the refinement of the mechanism of magnetic agglomeration, the results have an important theoretical reference value.

**Keywords:** rotating magnetic field, magnetic particles, dynamics, magnetic agglomeration, 3D finite element method

### 1. Introduction

Characterized by co-association of various minerals that are complex and difficult to separate, iron ore resources in China are generally of low overall grade. The sustainable development of iron ore resources is imminent, and the improvement of their utilization is imperative (Liu and Jin, 2009; Zhang et al., 2016). Magnetic agglomeration is widely present in the magnetic separation process. This agglomeration can capture non-magnetic or weakly magnetic particles, leading to a significant reduction in concentrate grade. This phenomenon exerts a significant influence on the processes of grinding, classification, separation, dewatering, and filtration (Ku et al., 2021; Ku et al., 2015; Xue et al., 2022; Yi et al., 2022).

Significant advancements have been achieved in rotating field magnetic separation technology and magnetic agglomeration theory due to the progress made in magnetic separation theory. Since the 1970s, domestic and foreign experts have studied the interactions between magnetic particles based on various theories such as the classical DLVO theory (Svoboda et al., 1987), Coulomb's law (J, 1984), and the loop current hypothesis (Okada et al., 1991). However, these studies rely solely on formulaic calculations or theoretical derivations to draw conclusions, which often differ significantly from the actual situation. Subsequently, the magnetic dipole theory (Encinas-Oropesa et al., 2001; Du and Du, 2006; Tartakovskaya, 2010; Zhao and Peng, 2012; Alqadi and Alzoubi, 2014) was employed to construct a magnetic dipole model for studying particle interactions (Yang et al., 2021), resulting in significant advancements in theoretical studies.

In recent years, research on the interaction between magnetic particles has progressed from theoretical derivation to simulation (Ji et al., 2016). Experts have utilized simulation models to conduct more in-depth and precise studies on the interaction between magnetic particles (Ntallis and Efthimiadis, 2014; Zeng et al., 2020; Xu et al., 2023; Liu et al., 2023; Yi et al., 2023; Zheng et al., 2023). However, the study of the dynamic process of magnetic agglomeration for magnetic particles is mostly based on simplifying magnetic particles to a 2D circular surface. During the running of a simulation, a 2D circular surface can be considered as a 3D column. There is a substantial distinction between a cylinder and a sphere. This dissimilarity may cause the simulation results to be less accurate or even contradictory to the actual situation.

In this study, a 3D finite element model is established to accurately simulate the motion and interaction of magnetic particles in a rotating magnetic field. Based on the simulation results, we analyzed the dynamic process of magnetic agglomeration of magnetic particles and further improved the magnetic agglomeration theory. We also provided theoretical references for optimizing and improving magnetic separation equipment, as well as for the development of new technologies.

## 2. Theories and Models

### 2.1 Theories

#### 2.1.1 Magnetic force $F_m$

In this paper, magnetic spherical particles are considered homogeneous and incompressible, and the "internal stress" of the spheres is not considered. In combination with Gauss theorem, the magnetic force is calculated using the surface force of Maxwell surface stress tensor method, as follows (Yamaguchi et al., 2010; Reyne et al., 1988):

$$F_m = \oint \left[ (\mathbf{B} \cdot \mathbf{n}) \mathbf{H} - \frac{1}{2} \mathbf{B} \mathbf{H} \mathbf{n} \right] dS \quad (1)$$

$$\frac{dF_m}{dS} = H_1 (B_1 \cdot \mathbf{n}) - \left( \frac{H_1 B_1}{2} \right) \mathbf{n} - \left[ H_2 (B_2 \cdot \mathbf{n}) - \left( \frac{H_2 B_2}{2} \right) \mathbf{n} \right] \quad (2)$$

where  $\oint$  is the closed area fraction,  $m^2$ ;  $\mathbf{B}$  is the magnetic flux density of the particle, T;  $\mathbf{n}$  is the unit normal vector pointing out of the surface, dimensionless;  $\mathbf{H}$  is the magnetic field strength, A/m;  $S$  is the surface area of the particle,  $m^2$ ; and the tensor  $T_m$  is expressed as follows (Reyne et al., 1988; Reyne et al., 1987):

$$T_m = dF_m/dS = \begin{bmatrix} B_1 H_1 - \frac{1}{2} \mathbf{B} \mathbf{H} & B_2 H_1 & B_3 H_1 \\ B_1 H_2 & B_2 H_2 - \frac{1}{2} \mathbf{B} \mathbf{H} & B_3 H_2 \\ B_1 H_3 & B_2 H_3 & B_3 H_3 - \frac{1}{2} \mathbf{B} \mathbf{H} \end{bmatrix} \quad (3)$$

where  $T_m$  is the magnetic tensor, N/m<sup>2</sup>;  $B_1, B_2, B_3$  are the components of the magnetic flux density  $\mathbf{B}$  of the particle in the X, Y, and Z directions, T, respectively;  $H_1, H_2, H_3$  are the components of the magnetic field strength  $\mathbf{H}$  of the particle in the X, Y, and Z directions, A/m, respectively.

#### 2.1.2. Magnetic agglomeration force $F_{mm}$

During the simulation, the magnetic agglomeration force is equal to the difference between the total magnetic force and the magnetic force of a single particle in the magnetic field. The expression for the magnetic agglomeration force on particle A is as follows:

$$F_{mm} = F_{m-BA} - F_{m-A} \quad (4)$$

where  $F_{m-A}$  is the magnetic force acting on particle A when particle A is alone in the magnetic field;  $F_{m-BA}$  is the magnetic force of the total magnetic field acting on particle A, when particle B enters the magnetic field with particle A.

#### 2.1.3. Effective gravity $G$

The particles are subjected to gravity and buoyancy in a fluid medium, with these two forces being equated to the effective gravity  $G$ :

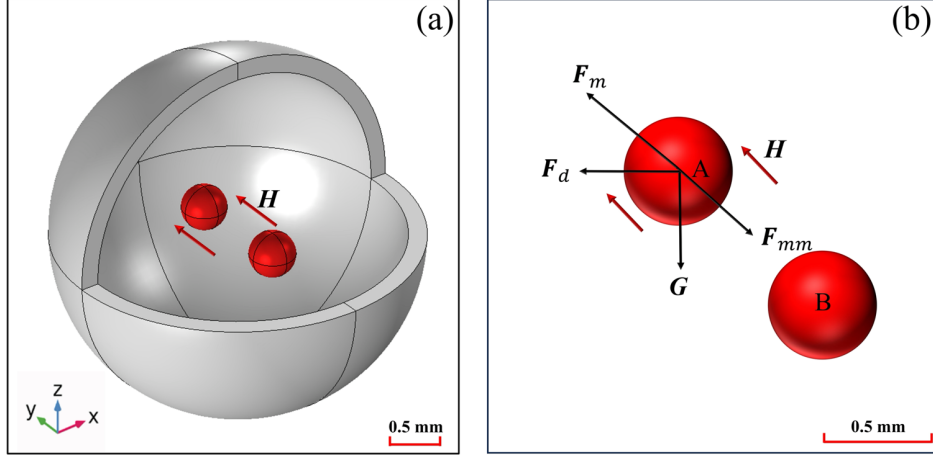


Fig. 1. (a) Spatial position of the particles, (b) analysis of particle forces.

$$G = \int_V (\rho_m - \rho_{fluid}) g dV \quad (5)$$

where  $\int_V$  is the closed volume fraction,  $m^3$ ;  $\rho_m$ ,  $\rho_{fluid}$  are the magnetic particle density and fluid medium density,  $kg/m^3$ , respectively;  $g$  is the acceleration of gravity,  $m/s^2$ .

#### 2.1.4. Fluid resistance $F_d$

The analysis of particle forces is illustrated in Fig. 1(b). According to the Navier-Stokes equations (N-S equations), the fluid is set to be isothermal and there is no change in energy. Therefore, the N-S equation expressions include only the mass conservation equation and the momentum conservation equation:

$$\frac{\partial \rho_{fluid}}{\partial t} + \nabla \cdot (\rho_{fluid} \cdot \mathbf{u}) = 0 \quad (6)$$

$$\rho_{fluid} \frac{\partial \mathbf{u}}{\partial t} + \rho_{fluid} (\mathbf{u} \cdot \nabla) \mathbf{u} = -\nabla p + \mu \nabla^2 \mathbf{u} + \mathbf{F} \quad (7)$$

where  $t$  is the fluid resistance action time,  $s$ ;  $\mathbf{u}$  is the velocity of the fluid,  $m/s$ ;  $p$  is the pressure,  $Pa$ ;  $\mu$  is the dynamic viscosity of the fluid,  $Pa \cdot s$ ;  $\mathbf{F}$  is the applied volume force,  $N$ .

In the simulation, the fluid is incompressible flow and equation (6) can be simplified to the following equation:

$$\rho_{fluid} \nabla \cdot \mathbf{u} = 0 \quad (8)$$

The fluid resistance  $F_d$  is obtained from equations (7) and (8):

$$\mathbf{F}_d = -\mu \nabla^2 \mathbf{u} + \nabla p = \iint \mathbf{f}_d dS \quad (9)$$

The components  $f_{dx}$ ,  $f_{dy}$ , and  $f_{dz}$  of its force  $f_d$  per unit area in the right-angle coordinate system are as follows, respectively:

$$f_{dx} = -\mu \left( 2 \frac{\partial u}{\partial x} \mathbf{i} + \left( \frac{\partial u}{\partial y} + \frac{\partial v}{\partial x} \right) \mathbf{j} + \left( \frac{\partial u}{\partial z} + \frac{\partial w}{\partial x} \right) \mathbf{k} \right) + \frac{\partial p}{\partial x} \quad (10)$$

$$f_{dy} = -\mu \left( \left( \frac{\partial v}{\partial x} + \frac{\partial u}{\partial y} \right) \mathbf{i} + 2 \frac{\partial v}{\partial y} \mathbf{j} + \left( \frac{\partial v}{\partial z} + \frac{\partial w}{\partial y} \right) \mathbf{k} \right) + \frac{\partial p}{\partial y} \quad (11)$$

$$f_{dz} = -\mu \left( \left( \frac{\partial w}{\partial x} + \frac{\partial u}{\partial z} \right) \mathbf{i} + \left( \frac{\partial w}{\partial y} + \frac{\partial v}{\partial z} \right) \mathbf{j} + 2 \frac{\partial w}{\partial z} \mathbf{k} \right) + \frac{\partial p}{\partial z} \quad (12)$$

where  $u$ ,  $v$ ,  $w$  are the components of fluid velocity  $\mathbf{u}$  in the X, Y, Z directions in the right-angle coordinate system,  $m/s$ , respectively;  $\mathbf{i}$ ,  $\mathbf{j}$ ,  $\mathbf{k}$  are the normal vectors in the X, Y, Z directions in the right-angle coordinate system, respectively, dimensionless.

## 2.2. Model construction

The finite element analysis software COMSOL Multiphysics was used to construct a 3D finite element

model of magnetic particles moving in a rotating magnetic field. The roles of the modules in the model are shown in Table 1. The Free Tetrahedral Mesh is used to partition the particle area, fluid area, and infinite area for finite element analysis. The geometry of the model is shown in Fig. 2. The grid discretization effect is shown in Fig. 3.

Table. 1 The roles of the modules in the model

Module	Role
The magnetic field, no current(mfnc)	set the parameter properties of the rotating magnetic field
The laminar flow	set the fluid properties
The solid mechanics	set the particle boundary load
The multi-physics field coupling	couple the multi-physics field with the solid particles

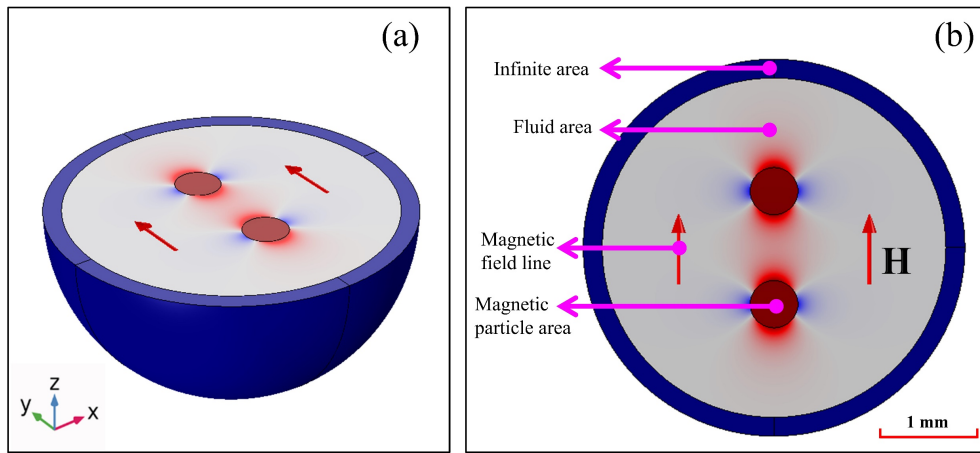


Fig. 2. 3D finite element simulation model. (a) 3D finite element model, (b) X-Y plane

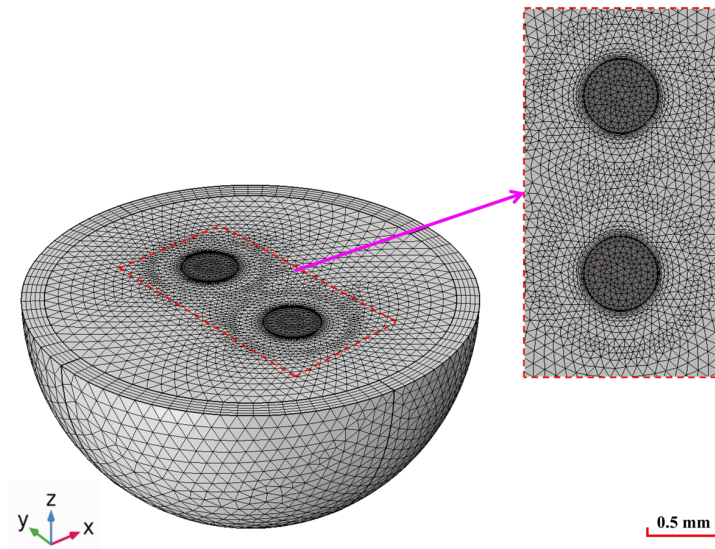


Fig. 3. Grid distribution in the computational domain

### 2.3. Rotating magnetic field and solver setup

In the process of simulating a magnetic field, the magnetic field, no current module satisfies the following equation:

$$H = -\nabla V_m + H_b \quad (13)$$

$$\nabla \cdot \mathbf{B} = 0 \quad (14)$$

where  $V_m$  is the magnetic scalar potential, A;  $H_b$  background magnetic field strength, A/m.

Setting the background magnetic field solution type as a Reduction Field. The component of  $H_b$  in the X and Y directions  $H_{bx}$ ,  $H_{by}$  are as follows:

$$H_{bx} = H_0/\mu_0 \sin(2\pi t n_0) \quad (15)$$

$$H_{by} = H_0/\mu_0 \cos(2\pi t n_0) \quad (16)$$

where  $H_0$  is the magnitude of the background magnetic field, A/m;  $\mu_0$  is the vacuum permeability,  $4\pi \times 10^{-7}$  H/m;  $t$  is the time of magnetic field operation, s;  $n_0$  is the magnetic field rotational speed, r/s. The magnetic flux is conserved throughout the solution domain, satisfying the following intrinsic relationship:

$$\mathbf{B} = \mu_0 \mu_r \mathbf{H} \quad (17)$$

where  $\mu_r$  is the relative magnetic permeability of the particle, dimensionless. The initial value of the magnetic scalar potential is set to zero:

$$V_m = 0 \quad (18)$$

### 3. Results and discussion

In order to explore the effects of different conditions, four models are constructed in this study, and some important parameters are shown in Table 2. Model NO.1 mainly explores the effect of the change of rotational speed of the rotating magnetic field. Model NO.2 explores the effect of the background magnetic field strength on the motion of the particles. Model NO.3 investigates the effect of the viscosity of the medium. Model NO.4 investigates the effect of the initial spacing between the two particles.

#### 3.1 Effect of different magnetic field rotational speeds (Model No. 1)

The parameter settings of the models are shown in Table 2. As shown in Fig. 4, we set the particle trajectory to rotate  $360^\circ$  along the tangent direction of the curve in one spiral as one cycle and label it with I, II, III. We call the vertical distance between two spirals the pitch. Let the time from the initial relative position of particles to the occurrence of agglomeration be  $t_a$ . In Fig. 5,  $V_X$  increases along the positive direction of the Y-axis, then decreases to 0, and then increases along the negative direction of the Y-axis before decreasing to 0. We refer to this change as one cycle. In contrast,  $V_Y$  increase along the Y-axis, decreases to 0, and then increases in the Y-axis direction to 0. Note this change as a cycle. In Fig. 6,  $a_X$  rises along the positive direction of the Y-axis before falling to 0. Then it increases along the negative direction of the Y-axis before falling back to 0. One cycle represents this shift. Acceleration  $a_Y$  is shown to increase to its maximum value and then decrease to its minimum, recording this change as a cycle.

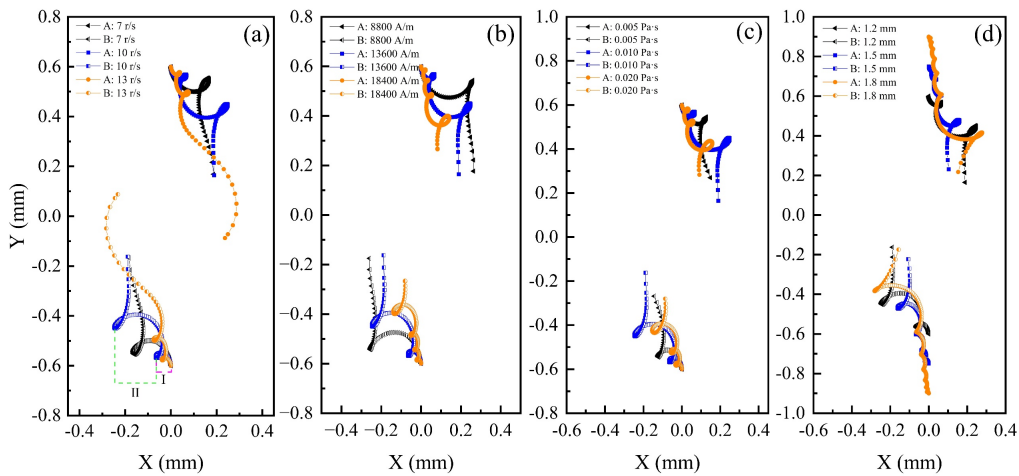


Fig. 4. Trajectories of particles A and B at different conditions, (a) different magnetic field rotational speeds, (b) different magnetic field strengths, (c) different viscosity media, (d) different initial spacing

Table 2. The parameter settings of models

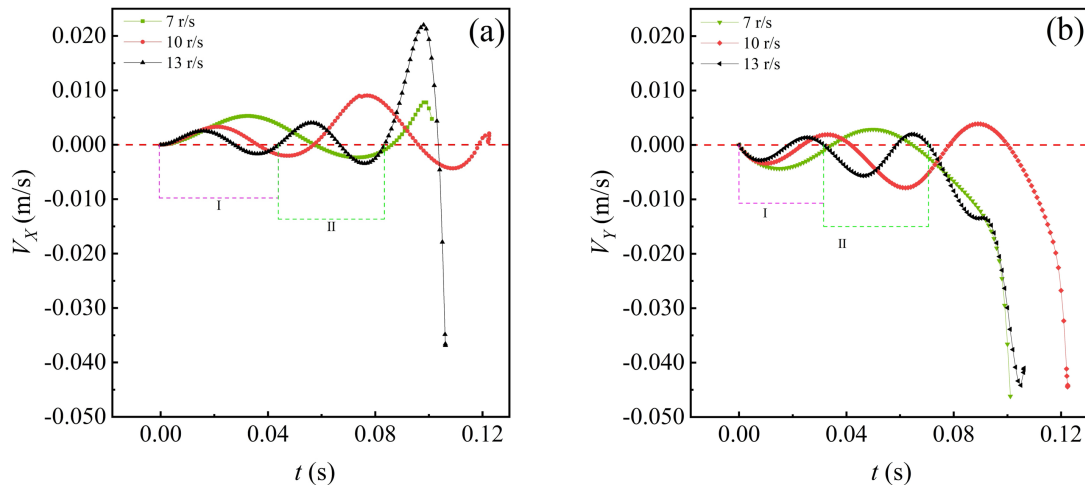
Model Variability	No. 1	No. 2	No. 3	No. 4
magnetic field rotational speeds $n$ (r/s)	7 10 13	10	10	10
magnetic field strength $H$ (A/m)	13600	8800 13600 18400	13600	13600
medium viscosity $\eta$ (Pa·s)	0.010	0.010	0.005 0.010 0.020	0.010
initial particle spacing $l_0$ (mm)	1.2	1.2	1.2	1.2 1.5 1.8
particle diameter $d$ (mm)	0.5	0.5	0.5	0.5

Table 3 shows that the periods of trajectory, velocity, and acceleration remain the same under different conditions. From Fig. 4, we can see that the trajectory of the particles is a center-symmetric spiral curve in the rotating magnetic field. The primary reason for the spiral in the particle trajectory is that the rotating magnetic field induces inconsistent changes in the forces acting on the particles in the X and Y directions. This leads to varying displacements, velocities, accelerations, and other characteristics of the particle motion, ultimately forming a spiral trajectory. Although the number of complete cycles is 2 when the magnetic field speed is increased to 13 r/s, the trajectories gyrate before the particle agglomeration, the actual period is 2.5, as shown in Fig. 4(a). The number of cycles grows with the magnetic field's rotational speed. The variation of  $t_n$  with magnetic field speed is insignificant.

Fig. 4(a) shows that the helical diameter and pitch of the particle trajectories increase in different cycles with increasing motion time at the same magnetic field rotational speed. The reason may be as follows: the Magnitude of magnetic force values on the particles unchanged in a rotating magnetic field. However, as the rotational speed of the magnetic field increases, the duration of the magnetic force is shortened, resulting in a decrease in particle displacement, pitch, and helix diameter. Conversely, at the same rotational speed, an increase in the duration of motion extends the duration of the magnetic force's action, leading to an increase in particle displacement, pitch, and helix diameter.

In Fig. 5, the maximum value of  $V_X$  increases with the increase of the magnetic field rotation speed, while the maximum value of  $V_Y$  has no obvious relationship with the magnetic field rotation speed.

As shown in Fig. 6, When  $t = 0$ ,  $a_X = 0$ , and  $a_Y$  has no obvious relationship with the speed of the magnetic field. The initial acceleration of the particles has no obvious relationship with the speed of the

Fig. 5. Velocity components  $V_X$ ,  $V_Y$  of particle A at different magnetic field rotational speeds

magnetic field. The magnetic force, magnetic agglomeration force and fluid resistance of the particles change periodically in the rotating magnetic field. The force on the particles in the initial state is not affected by the rotation speed of the magnetic field, but the acting time of the particles is negatively correlated with the rotation speed of the magnetic field. Therefore, the maximum value of particle acceleration and the total movement time in the first week have little change, but with the increase of the rotation speed of the magnetic field, the time for the particles to complete a cycle is shortened, and the number of particle movement cycles increases within the same total movement time.

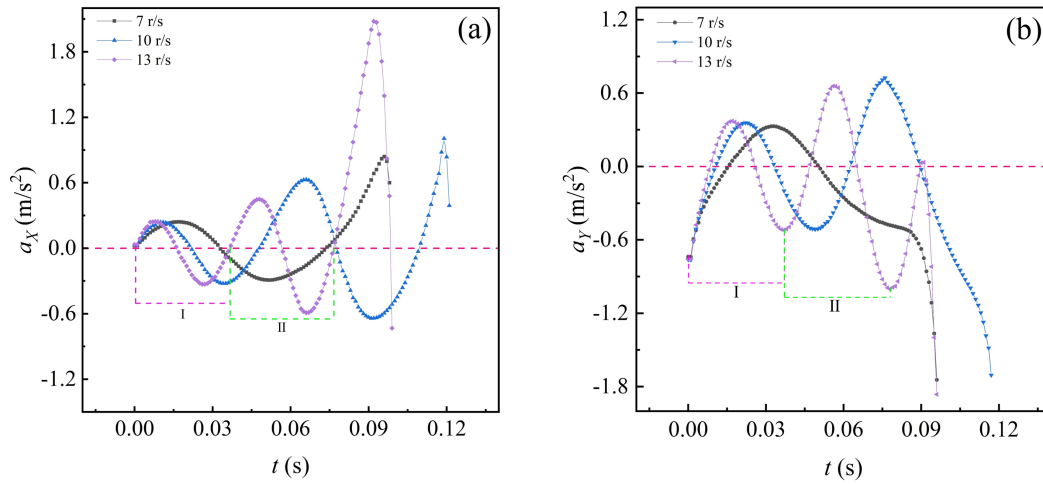


Fig. 6. Acceleration component  $a_x$ ,  $a_y$  of particle A at different magnetic field rotational speeds

Table 3. Complete cycles and  $t_a$  in various variables

Model	Item	Variability	Complete cycle number	$t_a^*$ (s)
No. 1	$n$ (r/s)	7	1	0.101
		10	2	0.123
		13	2	0.106
No. 2	$H$ (A/m)	8800	4	0.213
		13600	2	0.123
		18400	1	0.076
No. 3	$\eta$ (Pa·s)	0.005	1	0.007
		0.010	2	0.123
		0.020	3	0.162
No. 4	$l_0$ (mm)	1.2	2	0.123
		1.5	4	0.214
		1.8	7	0.366

$t_a^*$ : The time from the initial relative position of particles to the occurrence of agglomeration

### 3.2. Effect of different magnetic field strengths (Model No. 2)

From model No. 2 in Table 3, the number of periods of the trajectory, velocity, and acceleration are negatively correlated with the magnetic field strength. It was observed that  $t_a$  is negatively correlated with the magnetic field strength. With the increase in magnetic field strength, the total time of particle motion is shortened, and the number of particle motion cycles decreases.

As seen from Fig. 4(b), the pitch and helix diameter increase in the same cycle as the magnetic field strength increases, and they also increase simultaneously as the particle motion time increases at the same magnetic field strength. The reason may be that as the magnetic field strength increases, the magnetic force on the particles also increases, and the mutual attraction between the particles is enhanced. At the same magnetic field strength, as the time of particle motion increases, the time of

magnetic force action is prolonged, and the pitch, helix diameter increase.

In Fig. 7, The maximum value of  $V_X$  increases with the increase of the magnetic field intensity, and the maximum value of  $V_Y$  in the first cycle is positively correlated with the magnetic field intensity. In Fig. 8, during the first cycle, the maximum values of  $a_X$  and  $a_Y$  increase with the increase of magnetic field strength. The reason is that the magnitude of the magnetic force and magnetic agglomeration force on the particle in its initial state increases with an enhancement in the magnetic field strength.

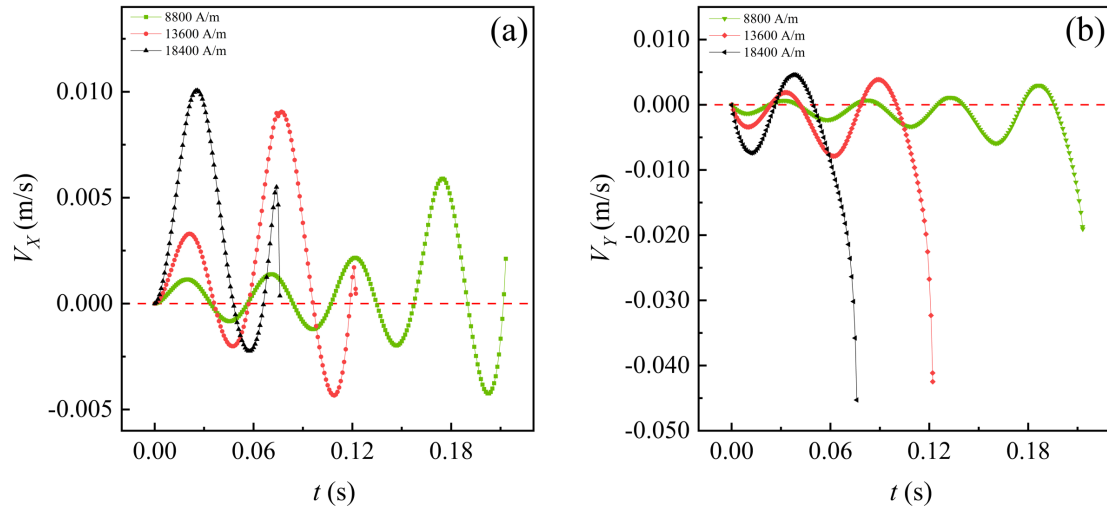


Fig. 7. Velocity component  $V_X$ ,  $V_Y$  of particle A at different magnetic field strengths

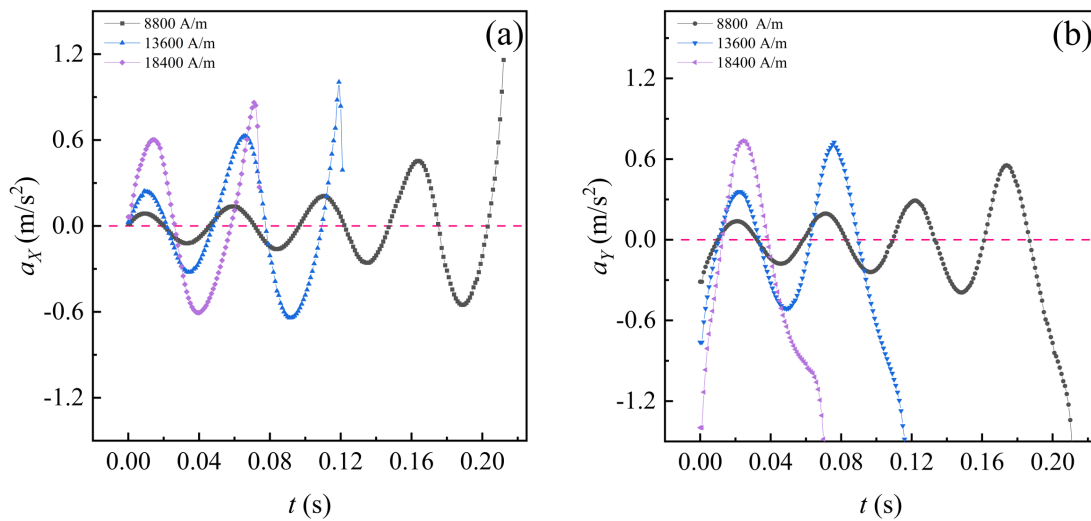


Fig. 8. Acceleration component  $a_X$ ,  $a_Y$  of particle A at different magnetic field strengths

### 3.3. Effect of viscosity of different media (Model No. 3)

From model No. 3 in Table 3, the relationship between the medium viscosity and the number of periods of the trajectory, velocity, and acceleration is positive. And  $t_a$  is positively correlated with the medium viscosity. Fig. 4(c) shows that with the viscosity of the medium increasing, the pitch and spiral diameter in the same cycle all decrease, but increase as the particle motion time increases at the same medium viscosity. They are negatively correlated with medium viscosity and positively correlated with motion time. As the viscosity of the medium increases, the resistance of the fluid to the particles also increases, leading to a weakening of the mutual attraction between the particles. As the time of particles movement increases, the magnetic agglomeration force between them gradually increases, while the influence of fluid resistance on the particles gradually decreases, causing the pitch and spiral diameter to increase.

As can be seen from Fig. 9, The maximum values of  $V_X$  and  $V_Y$  are negatively correlated with the

viscosity of the medium in the first cycle. In Fig. 10, the maximum acceleration values exhibit an insignificant negative connection with the medium viscosity during the first cycle. Additionally, the time it takes to reach the maximum value for  $a_X$  and  $a_Y$  is negatively correlated with the viscosity of the medium. And  $a_Y$  falls as the viscosity of the medium grows, at  $t = 0$ ,  $a_X = 0$ . The initial acceleration magnitude is negatively correlated with medium viscosity. The medium viscosity of the fluid affects the resistance of the fluid to the motion of particles. As the medium viscosity increases, the fluid resistance also increases. Additionally, an increase in medium viscosity prolongs the total time of particle motion and increases the number of cycles of particle motion.

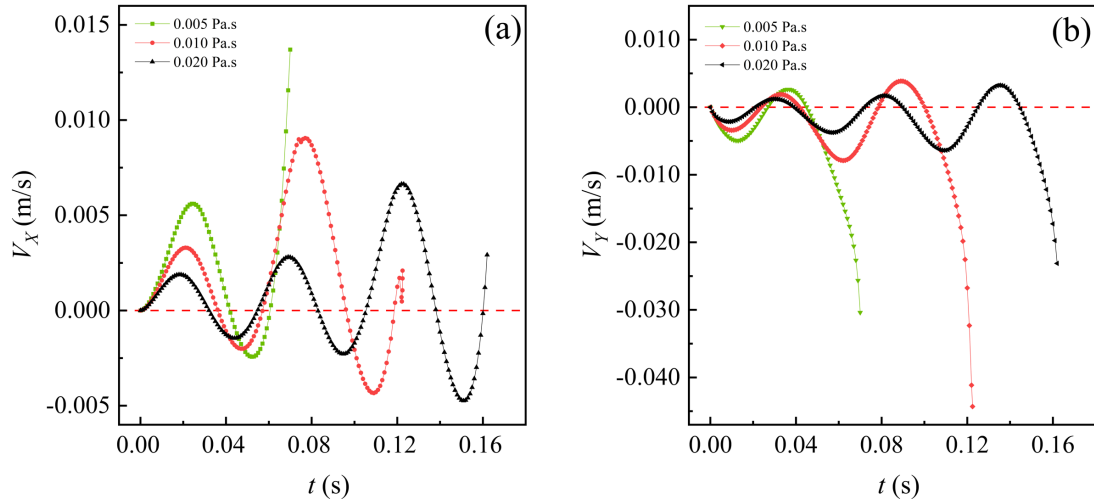


Fig. 9. Velocity components  $V_X$ ,  $V_Y$  of particle A at different medium viscosities

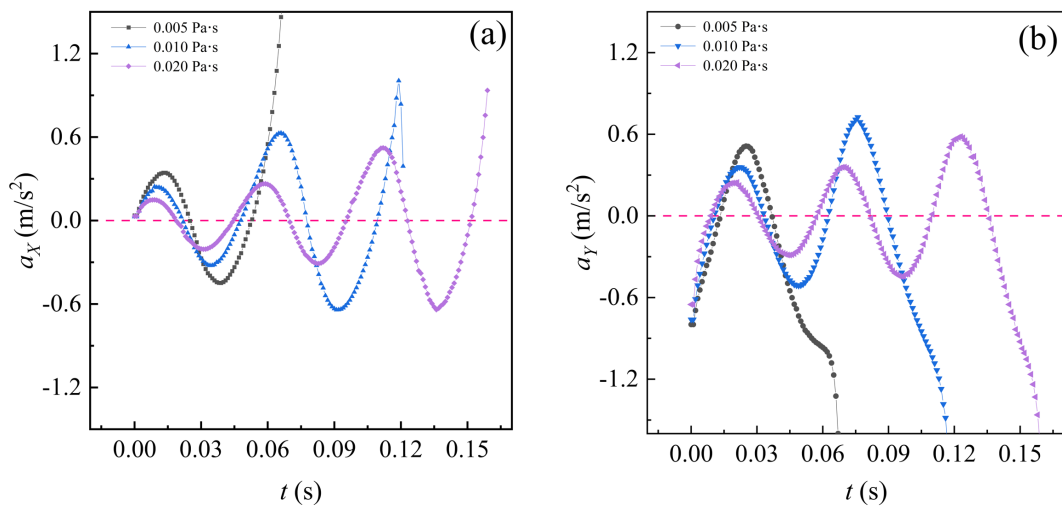


Fig. 10. Acceleration component  $a_X$ ,  $a_Y$  of particle A at different medium viscosities

### 3.4. Effect of different initial spacing (Model No. 4)

As can be seen from model No. 4 in Table 3, the number of periods is positively correlated with the initial spacing of particles. And  $t_a$  is prolonged with the increase in the initial particle spacing. Fig. 4(d) shows that as the initial spacing between the particles increases, the motion of the particles in the X-direction before agglomeration gradually changes to a small oscillation. One possible explanation for this phenomenon is that the strength of the interaction between two particles diminishes as the initial distance between the particles increases. At this time, the motion of the particles is mainly influenced by the magnetic force and the fluid resistance. As the particles continue their motion and approach each other, the magnetic agglomeration force between them gradually intensifies, and its influence on particle motion also increases gradually.

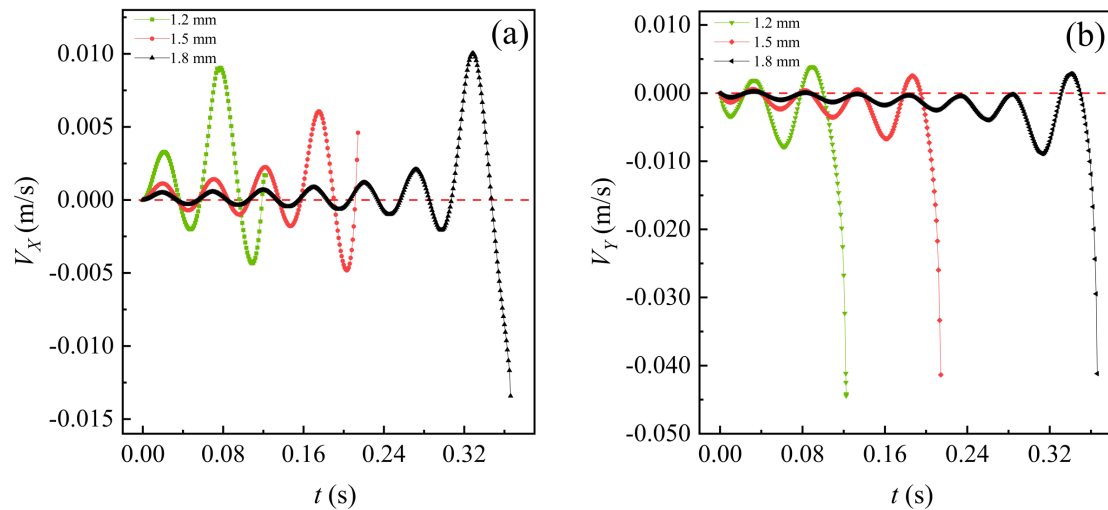


Fig. 11. Velocity components  $V_X$ ,  $V_Y$  of particle A at different initial pitches

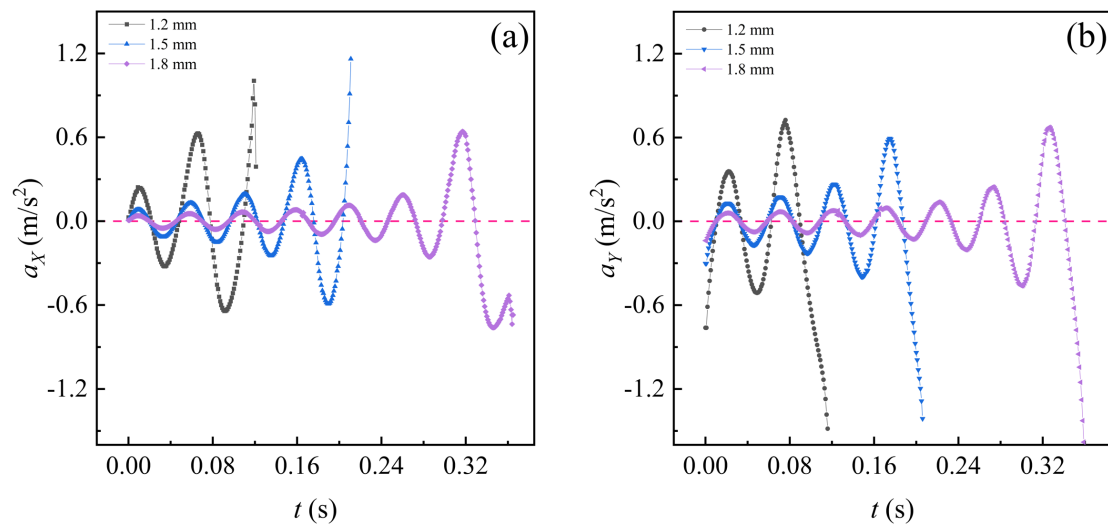


Fig. 12. Acceleration component  $a_X$ ,  $a_Y$  of particle A at different initial pitches

In Fig. 11,  $V_Y$  increases drastically along the negative vertical direction at the end of the integer cycle. As the initial distance between particles increases, initial interaction weakens, resulting in a deceleration of particle agglomeration and an increase in the number of movement cycles. When the particles move to a certain distance, they rapidly approach, and agglomeration occurs. As can be seen from Fig. 12, the acceleration  $a_X = 0$  at  $t = 0$ . The magnitude of the acceleration  $a_Y$  decreases with the increase of the initial distance. This phenomenon can be attributed to the fact that the magnitude of the magnetic force and magnetic agglomeration force on the particle in the initial state decreases with the increase in the initial distance, but the time of action of the force remains essentially the same. Therefore, in the first cycle, the particle acceleration maximum is negatively correlated with the initial distance.

#### 4. Conclusions

- (1) The trajectory of two particles is a centrosymmetric periodic spiral curve in the rotating magnetic field. The periods of particle trajectories exhibit a positive correlation with magnetic field speed, medium viscosity, and initial particle spacing while displaying a negative correlation with magnetic field strength. The time of particle movement shows a negative relationship with the strength of the magnetic field, a positive relationship with the viscosity of the medium and the initial spacing between particles.
- (2) The velocities of the particles in X and Y directions are periodically varying, and their period number

changes are consistent with the period number changes of the particle trajectory and acceleration. The period number changes of  $V_x$  and  $V_y$  are consistent with the period number changes of the trajectory and acceleration.

- (3) The initial acceleration is positively correlated with the magnetic field strength, negatively correlated with the medium viscosity and initial spacing, and has no significant relationship with the magnetic field speed.
- (4) In the rotating magnetic field, appropriately increasing the magnetic field speed and decreasing the magnetic field strength can help increase the number of particle aggregation-dispersions and slow down the particle magnetic agglomeration process. Increasing the viscosity of the fluid medium and particle spacing helps to increase the oscillation of particles in the fluid medium, which is beneficial to remove inclusions in magnetic agglomeration.

### Acknowledgments

The work was supported by National Natural Science Foundation of China under Grant 52174245, Natural Science Foundation of Fujian Province under Grant 2021J01552 and Open Foundation of the State Key Laboratory of Mineral Processing (Nos. BGRIMM-KJSKL-2021-02 and BGRIMM-KJSKL2022-03).

### References

- ALQADI, M.K., ALZOUBI, F.Y., 2014. *Magnetic interaction in the metamaterial/magnet system*. Chin. Phys. B.
- DU A, DU H 2006. *Monte Carlo calculation of the magnetization behavior and the magnetocaloric effect of interacting particles*. J. Magn. Magn. Mater., 299, 247-254.
- ENCINAS-OROPESA, A, DEMAND, M, PIRAUX, L, et al., 2001. *Effect of dipolar interactions on the ferromagnetic resonance properties in arrays of magnetic nanowires*. J. Appl. Phys., 89, 6704-6706.
- J C L 1984. *Improving the way of magnetic separation of fine-grained magnetite (in Chinese)*. Metal Mine, 43-46.
- Ji, B., WU, P., REN, H., et al. 2016. *Segregation behavior of magnetic ions in continuous flowing solution under gradient magnetic field*. Chin. Phys. B, 25, 74704-074704.
- KU, J., CHEN, H., HE, K., et al. 2015. *Force analysis and dynamic simulation of ferromagnetic mineral particles in magnetic separation process*. Journal of Central South University (Science and Technology), 46, 1577-1582.
- KU, J., XIA, J., LI, J., et al. 2021. *Accurate calculation of major forces acting on magnetic particles in a high-gradient magnetic field: A 3D finite element analysis*. Powder Technol., 394, 767-774.
- LIU, J., JIN, S., 2009. *The actuality and counter measure of the iron ore resource in China*. China Mining Magazine, 18, 1-2, 19.
- LIU, J., XIE, S., LI, X., et al. 2023. *Separating efficiency of ferromagnetic particles and principle of low-intensity dry magnetic separator under different air supply modes: Based on multi-physical modeling*. Powder Technol., 415, 118155.
- NTALLIS, N., EFTHIMIADIS, K.G., 2014. *A 3D finite elements micromagnetic simulation of a ferromagnetic particle*. J. Magn. Magn. Mater., 363, 152-157.
- OKADA, I., OZAKI, M., MATIJEVIĆ, E. 1991. *Magnetic interactions between platelet-type colloidal particles*. J. Colloid Interface Sci, 142, 251-256.
- REYNE, G., SABONNADIÈRE, J., COULOMB, J., et al. 1987. *A survey of the main aspects of magnetic forces and mechanical behaviour of ferromagnetic materials under magnetization*. IEEE T Magn., 23, 3765-3767.
- REYNE, G., SABONNADIÈRE, J., IMHOFF, J., 1988. *Finite element modelling of electromagnetic force densities in DC machines*. IEEE T Magn., 24, 3171-3173.
- SVOBODA, J., LAZER, M., RIELE, W.T., 1987. *Selective magnetic separation of uranium and gold*. IEEE T Magn., 23, 283-293.
- TARTAKOVSKAYA, E.V., 2010. *Reorientation phase transitions in planar arrays of dipolarly interacting ferromagnetic particles*. J. Magn. Magn. Mater., 322, 3495-3501.
- XU, Z., TANG, Z., CHEN, F., et al. 2023. *Study of lateral assembly of magnetic particles in magnetorheological fluids under magnetic fields*. J. Magn. Magn. Mater., 566, 170293.
- XUE, Z., WANG, Y., ZHENG, X., et al. 2022. *Role of gravitational force on mechanical entrainment of nonmagnetic particles in high gradient magnetic separation*. Miner. Eng, 186, 10772.
- YAMAGUCHI, M., OZAWA, S., YAMAMOTO, I., 2010. *Dynamic Behavior of Magnetic Alignment in Rotating Field for*

- Magnetically Weak Particles.*, Jpn. J. Appl. Phys., 49, 080213.
- YANG, Y., YANG, S., YANG, W., et al. 2021. *Angular dependence of vertical force and torque when magnetic dipole moves vertically above flat high-temperature superconductor.* Chin. Phys. B, 30, 571-576.
- YI, F., CHEN, L., ZENG, J., 2023. *Combinatorial optimization of rotating matrix in centrifugal high gradient magnetic separation.* Miner. Eng., 202, 108309.
- YI, F., CHEN, L., ZENG, J., et al. 2022. *Rotating flow characteristics in centrifugal high gradient magnetic separation and its effect on particle capture behavior.* Miner. Eng., 179, 107442.
- ZENG, J., TONG, X., XU, G., et al. 2020. *Comparative magnetic capture characteristics of revolving and spinning wires in uniform magnetic field.* Powder Technol., 363, 161-168.
- ZHANG, L., YANG, H., FENG, A., et al. 2016. *Study on Utilization and Analysis of Supply and Demand of Global Iron Ore resources.* Conservation and Utilization of Mineral Resources, 57-63.
- ZHAO, C., PENG, X. 2012. *Analysis of properties of magnetorheological fluids calculated by finite element method and comparison with results based on magnetic dipole model.* Journal of Functional Materials, 43, 2098-2101.
- ZHENG, X., LI, S., DU, L., et al. 2023. *Investigation of particle capture by grooved plates with elliptic teeth for high intensity magnetic separation.* Sep. Purif. Technol., 325, 124685.